Journal of Catalysis **205,** 177–190 (2002)
doi:10.1006/jcat.2001.3416, available online at http://www.idealibrary.com on IDEAL®

Theoretical Analysis of CO Adsorption on the Reduced Cr/Silica System

Øystein Espelid and Knut J. Børve[1]

Department of Chemistry, University of Bergen, Allégaten 41, N-5007, Bergen, Norway

Received July 4, 2001; revised September 12, 2001; accepted September 12, 2001

Cluster models are constructed for mononuclear Cr(II) and Cr(III) sites as well as dinuclear Cr(II) sites of the reduced Cr/SiO_2-based Phillips catalyst. The binding energies and structures of oligocarbonyl complexes formed at these cluster models have been computed using density functional theory. Furthermore, harmonic frequencies and infrared intensities are calculated for the carbonyl stretching modes of these complexes. The resulting parameters are compared to literature spectra of CO-exposed Phillips catalysts and related model systems. A reassignment is proposed for the infrared spectrum of carbon monoxide on the reduced Cr/silica system.

Key Words: **carbon monoxide; adsorption; infrared spectroscopy; Phillips catalyst; density functional theory; cluster models.**

1. INTRODUCTION

Vibrational spectroscopy of adsorbed probe molecules has proven to be a powerful technique for characterizing supported metal-based catalysts, both with respect to acidity and coordination environment (1, 2). In the context of Phillips catalysis for polymerization of ethylene (3), at the focus of this communication, both ammonia and various diatomic gases (N_2, NO, CO) have been used as adsorbates. Infrared spectroscopy of chromium–carbonyl species holds a unique position in research on the reduced Phillips system. In fact, Ghiotti *et al.* (4) were able to discriminate between Cr(II) species differing only in their degree of coordinative unsaturation, and other researchers were able to reach conclusions regarding the nuclearity and oxidation state of chromium in these systems (5). Despite the application of advanced spectroscopy for over more than two decades, a unifying picture of the microscopic composition of Phillips-type catalysts is still wanting (6).

At the core of the Phillips process are supported chromium oxide catalysts, prepared industrially by impregnating a chromium compound onto wide-pore silica (7). In the calcined catalyst, chromium is in its hexavalent state, either predominantly as monochromate species, e.g., on pyrogenic silica at low chromium loadings, or as both dichromate and monochromate, as found on industrial sol–gel silica (6). The catalyst is reduced before attaining full activity, either during the early stages of contact with ethylene or in a separate pretreatment step, by exposing the catalyst to carbon monoxide at elevated temperatures (7). It is widely believed that after reduction, the dominating chromium species is divalent (6), with the remaining chromium present as unreactive chromia particles (8) or as isolated Cr(III) species (9).

Infrared (IR) spectroscopy of adsorbed carbon monoxide has been used extensively to characterize the dilute, reduced Cr/Silica system. However, work done with different choices of silica support has led to two comprehensive interpretations of the IR spectra, with some notable discrepancies between them.

IR spectra of catalysts prepared on pyrogenic silica have been interpreted based on an assumption of mononuclear pseudo-tetrahedral Cr(II) as the totally dominating chromium species, differing only in their degree of coordinative unsaturation; A > B > C (4). When exposed to carbon monoxide, Cr(II)-A sites are proposed to adsorb three equivalents of CO and to give rise to bands in the high-frequency range of the IR spectrum. Conversely, each Cr(II)-B site is proposed to adsorb only one CO ligand, while Cr(II)-C sites are proposed inactive to CO adsorption at room temperature (4). Kohler and Ekerdt assigned the bands at 2178, 2191, and 2212 cm^{-1} to a *mer*-Cr(II)–$(CO)_3$ species of C_{2v} symmetry (10). Furthermore, a peak at 2184 cm^{-1} was assigned to a separate species. At low temperature, an increasing CO coverage is accompanied by the appearance of two intense peaks at 2100 and 2120 cm^{-1} as well as a broad and less intense band in the region of 2035–2045 cm^{-1} (11). These changes in the IR spectrum are not well understood.

IR spectroscopy of chromium–carbonyl species of catalysts prepared on sol–gel silica has lead to an interpretation that anticipates a population of both mono- and dinuclear species, with the two chromium atoms in the dinuclear site connected via an oxygen bridge (5). Carbon monoxide may coordinate to a dinuclear site in either terminal or bridging positions, due to the inherent closeness of the chromium atoms. The high-frequency bands (2178, 2184, 2191 cm^{-1})

[1] To whom correspondence should be addressed. Fax: (475) 558-9490. E-mail: knut.borve@kj.uib.no.

0021-9517/02 $35.00

are assigned to vibrations of terminal carbonyls of both mononuclear and dinuclear complexes, whereas the low-frequency bands (2045, 2100, 2120 cm^{-1}) are assigned to vibrations of bridging carbonyls (5).

As an alternative to adding an external reducing agent, the catalyst may be activated through heating under vacuum. Carbonyl IR spectra of a thus-activated catalyst were reported to show a triplet of bands positioned at 2202, 2214, and 2228 cm^{-1} (12), assigned by Zielinski *et al.* to carbonyl complexes of Cr(III) surface species (12). The most intense component of this triplet, shifted down by a couple of wave numbers from 2202 cm^{-1}, is observed at elevated CO pressure also when the catalyst is reduced in conventional ways, as a weak shoulder to the 2191-cm^{-1} band (5, 10, 11). However, there is disagreement with respect to the assignment, with suggestions covering CO adsorbed to both Cr(II)–C (11) and Cr(IV) (10) sites, in addition to Cr(III) sites (5, 13).

In summary, two partly conflicting interpretations of the carbonyl IR spectra exist in the literature, arrived at from studies of catalysts that differ with respect to the silica support. To some extent, conflicting assignments may be resolved by reference to differences in nuclearity of the chromium sites at the different kinds of silica (6). This applies, for instance, to the bands at 2178 and 2191 cm^{-1}, since it is conceivable that terminal CO may show up with the same frequency on both mono- and dinuclear Cr(II) sites. In other cases, since the same peaks arise in the spectra irrespective of the support material this indicates that they have the same origin independent of the silica used. Moreover, previous analyses have been made with little regard for disparity in the local geometry of mononuclear chromium bonded to the support, even though it is conceivable that this may influence adsorption capacity as well as vibrational frequencies of adsorbed carbonyl species.

The aim of the present work is to provide a theoretical framework for a unified analysis of carbonyl IR spectra of reduced Cr/SiO_2 catalysts. To this end, we have constructed cluster models of coordinatively unsaturated mononuclear and dinuclear Cr(II) sites and mononuclear Cr(III) sites. Quantum chemical modeling is subsequently used to compute the structure, stability, and vibrational frequencies of the corresponding carbonyl complexes. Based on this information, carbonyl IR spectra from the literature are partly reassigned and used to identify chromium sites at the catalyst.

2. COMPUTATIONAL MODELS

2.1. Cluster Models

The dominating mononuclear chromium species of the reduced catalyst is believed to be divalent and bound by two oxygen ester linkages to the surface. While an unstrained ∠OCrO bond angle of a reduced chromium surface species may be expected to lie in the vicinity of 150°, i.e., close to the

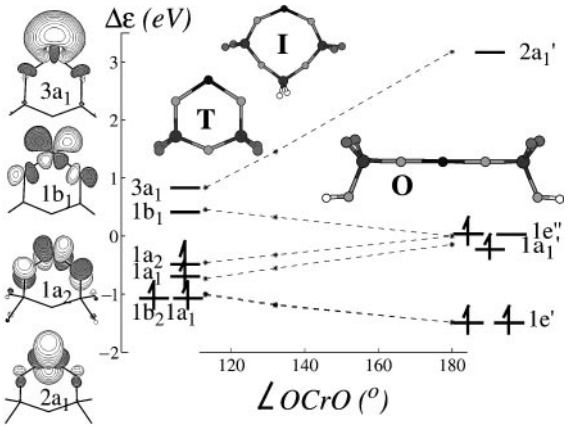

FIG. 1. Walsh diagram of the molecular orbitals with mainly Cr 3d and 4s character of divalent mononuclear chromium cluster models (**T**, **I**, **O**) with the ∠OCrO bond angle in the tetrahedral-to-octahedral range. The elements are coded on a gray scale according to increasing atom number, H (white) < O < F < Si < Cr (dark gray).

∠OCrO bond angle of $Cr(OH)_2(g)$ (14), the geometry realized at the silica surface depends also on the structure and flexibility of the anchoring site. Thus, one should consider a distribution of mononuclear Cr(II) surface species, characterized by the value of ∠OCrO. Here, this distribution is represented by three cluster models: a pseudo-tetrahedral cluster (**T**: $Cr(OSiF_2)_2O$, left in Fig. 1); a pseudo-octahedral cluster (**O**: $Cr(OSiF_2OH)_2$, right); and a cluster of intermediate ∠OCrO bond angle (**I**: $Cr(OSiF_2O)_2SiH_2$, center).

Depending on the load of chromium and the method of reduction, the reduced Cr/silica system may show substantial amounts of dinuclear chromium(II) and mononuclear chromium(III) species. They are modeled by clusters shown in Figs. 2 and 3, respectively. The two dinuclear chromium(II) cluster models may be regarded as an –OCrOCrO– moiety anchored to sites of narrow (**D_n**: $O(CrOSiF_2)_2O$) and intermediate-to-wide "bites" (**D_w**: $O(CrOSiF_2OH)_2$), similar to those of the mononuclear **T** and **O** cluster models, respectively. The Cr(III) cluster (**CrIII**) consists of chromium bound to a ring of three silanol moieties, themselves bound to one another through oxygen bridges. The molecular formula becomes $Cr(SiO_2F)_3$.

The **T**, **I**, **D_n**, and **CrIII** cluster models are identical to those used in a parallel study of electronic d–d transitions (15). Here, the set of surface models was expanded to include the **D_w** cluster, representing a dinuclear chromium species anchored at a surface site of wider bite. Furthermore, to increase compatibility within the set of clusters, the **O** cluster was terminated by two fluorine atoms and one hydroxyl moiety at each silicon. Details regarding the coordination sphere of chromium are included in Table 1 for later reference. To maintain a close-to-linear **O** cluster, the Si–Si distance was frozen at 6.9 Å, i.e., the equilibrium distance of the cluster as terminated by six fluorines and made

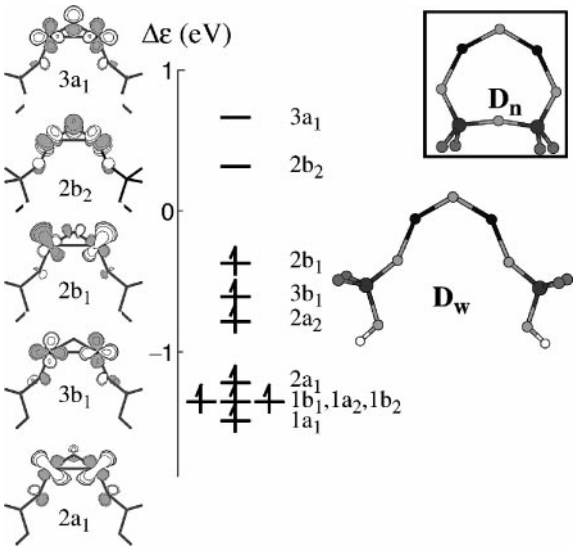

FIG. 2. Relative energy levels and isosurfaces of the molecular orbitals with mainly Cr 3d and 4s character of the dinuclear $\mathbf{D_w}$ cluster, as obtained with DFT-1. Also included are the structures of the dinuclear $\mathbf{D_w}$ and $\mathbf{D_n}$ (inserted) clusters. The elements are coded on a gray scale according to increasing atom number, H (white) < O < F < Si < Cr (dark gray).

subject to D_{3h} symmetry. Likewise, to maintain a wide-bite $\mathbf{D_w}$ cluster, the Si–Si distance was frozen at 7.0 Å. To prevent excessive geometric relaxation in these two clusters following adsorption of carbon monoxide, only chromium and oxygen atoms coordinating to chromium were allowed to relax geometrically.

2.2. *Calibration Study*

The bonds that form between carbon monoxide and transition metals pose a challenge to quantum chemical methods (17). Qualitatively, the metal–CO bond is usually described in terms of ligand-to-metal donation and metal-to-ligand back-donation, with 5σ and 2π (also denoted π^*) constituting CO's donating and accepting molecular orbitals, respectively. A quantitative description needs to include both of these aspects in an accurate and balanced way, which is difficult both to accomplish and to recognize when succeeded. The present study was conducted in terms of two different combinations of density functionals and atomic basis sets, referred to as DFT-1 and DFT-2 and detailed in the Appendix. Both methods are generally considered to be reliable and of useful accuracy, and this view is confirmed by their ability to describe relevant electronic properties of the separated CO and cluster entities (cf. Table 2).

It is evident that while DFT-1 systematically overestimates the bond lengths by ∼1 pm, both methods are able to reproduce the observed shifts in carbon–oxygen bond

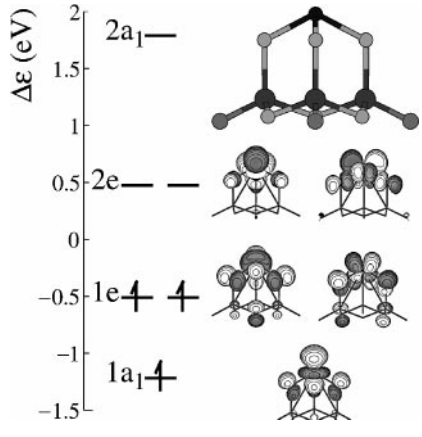

FIG. 3. Relative energy levels and isosurfaces of the orbitals with mainly Cr 3d and 4s character of the Cr(III) cluster (**CrIII**) as obtained with DFT-1. The elements are coded on a gray scale according to increasing atom number, O (light gray) < F < Si < Cr (dark gray).

TABLE 1

Selected Geometry Parameters of the Cluster Models: Tetrahedral (T), Intermediate (I), and Octahedral (O) Mononuclear Cr(II); Narrow-Bite ($\mathbf{D_n}$) and Wide-Bite ($\mathbf{D_w}$) Dinuclear Cr(II); and Mononuclear Cr(III) (CrIII)[a]

	State	rCrO	rSiO	∠OCrO	∠SiOCr
T	$^5B_1$	1.84	1.62	108	127
I	$^5B_1$	1.82	1.63	132	141
O	$^5B_1$	1.83	1.62	180	179
$\mathbf{D_w}$[b]	$^9A_2$	1.84	1.59	145	160
$\mathbf{D_n}$[b]	$^9A_2$	1.86	1.61	139	142
CrIII	$^4A_2$	1.81	1.65	104	114

[a] Units: bond length (r) in Å, angle (∠) in degrees.
[b] Geometry parameters unique to $\mathbf{D_w}$ and $\mathbf{D_n}$: $r\mathrm{CrO_{bridge}}$ $\mathbf{D_w}$: 1.77 Å, $\mathbf{D_n}$: 1.78 Å. ∠CrOCr $\mathbf{D_w}$: 123°, $\mathbf{D_n}$: 120°.

TABLE 2

Spectroscopic Properties of Carbon Monoxide and Mononuclear Cr(II) Clusters[a]

	DFT-1	DFT-2	Best value
CO $X\,^1\Sigma^+, r, \omega$	1.141, 2116	1.129, 2207	1.128, 2170[b]
CO a $^3\Pi_r, r, \omega$	1.217, 1718	1.205, 1778	1.206, 1743[b]
CO^+ $X\,^2\Sigma^+, r, \omega$	1.125, 2185	1.112, 2297	1.115, 2214[b]
CO a $^3\Pi_r \leftarrow X\,^1\Sigma^+, T_e$	5.71	5.82	6.04[b]
CO, ionization potential	14.04	14.17	14.01[b]
T $^5A_1 \leftarrow X\,^5B_1, T$	1.24	1.09	0.95[c]
T $^5A_2 \leftarrow X\,^5B_1, T$	1.05	1.11	1.04[c]
T $^5B_2 \leftarrow X\,^5B_1, T$	1.64	1.58	1.49[c]
O, Electron affinity	2.61	2.53	2.46[d]

[a] Units: bond length (r) in Å, harmonic frequency (ω) in cm^{-1}, and transition energy (T) and ionization potential in eV.
[b] Experimental, Ref. (16).
[c] *Ab initio* value, Ref. (15).
[d] Computed by means of CCSD(T) and extrapolated according to PCI-83.

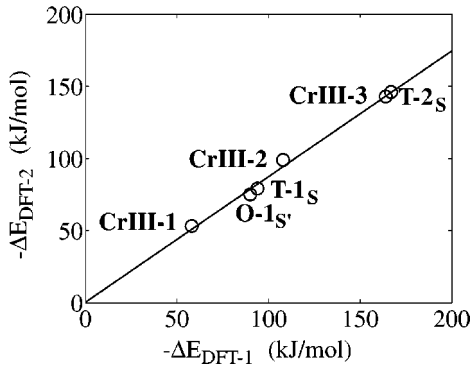

FIG. 4. Overall adsorption energies ($-\Delta E$) for six oligocarbonyl complexes at mononuclear clusters, as obtained with DFT-1 and DFT-2.

lengths upon excitation and ionization. The harmonic frequencies are predicted too low by DFT-1 and too high with DFT-2, thus bracketing the experimental values. This property is previously noted also for chromiumhexacarbonyl (18, 19) and other first-row transition-metal monocarbonyls (17).

The calibration study was continued by computing the stability of CO as adsorbed onto the **O** cluster, using a highly accurate *ab initio* method: CCSD(T) extrapolated according to PCI-83 (cf. Appendix). The coordination energy was found to be 80 and 85 kJ/mol in the geometries optimized by DFT-1 and DFT-2, respectively. (The **O** cluster was terminated by six fluorine atoms during the calibration study to increase the molecular symmetry.) From the energies, the adsorption geometry predicted by DFT-2 appears superior to that predicted by DFT-1. However, with respect to stability, the two DFT models lead to energies that bracket the more accurate estimate of 85 kJ/mol, at 92 kJ/mol (DFT-1) and 75 kJ/mol (DFT-2). Hence, provided that the DFT methods agree on the qualitative aspects of the metal–CO bond, an improved estimate of the true adsorption energy is apparently given by $-\Delta E = (-\Delta E_{\text{DFT-1}} - \Delta E_{\text{DFT-2}})/2$.

The two DFT models predict the same trend with respect to the coordination energies of higher carbonyls, (see Fig. 4). Based on the computed stability of six terminal Cr(II) and Cr(III) carbonyl complexes, we find $-\Delta E_{\text{DFT-2}} = 0.87 \times (-\Delta E_{\text{DFT-1}})$, with a correlation coefficient of $r^2 = 0.99$. Drawing on this correlation, one may replace averaging over the two methods by scaling; for example, $-\Delta E = 0.94 \times (-\Delta E_{\text{DFT-1}}) = 1.07 \times (-\Delta E_{\text{DFT-2}})$. These scaling factors will be used in isolated cases when a coordination step has been investigated using only one of the computational models.

3. RESULTS

3.1. Adsorption States and Stabilities

All the investigated chromium–carbonyl complexes are listed in Table 3, together with associated chromium–carbon distances and energy parameters. The symbol ΔE^1 is used to denote the reaction energy of

$$\vdash\text{Cr(CO)}_{m-1} + \text{CO}(g) \rightleftharpoons \vdash\text{Cr(CO)}_m, \qquad [1]$$

which describes the adsorption of one (additional) molecule of CO to chromium in a particular environment (denoted by $\vdash$Cr). By convention, the quantities "adsorption

TABLE 3

Chromium–Carbon Bond Lengths and Reaction Energies of Eq. [1] for the Last Added CO of Carbonyl Complexes at Cluster Models of Cr/Silica

	DFT-1			DFT-2	
Complex	ΔE^1 (kJ/mol)	ΔE^1 (kJ/mol)	rCr–C (Å)	ΔE^1 (kJ/mol)	rCr–C (Å)
T-1$_S$	−87[a]	−94	2.06	−79	2.13
T-2$_S$	−70[a]	−73	2.08	−67	2.15
T-2$_T$	−12[b]	−13	2.03		
T-3$_S$	−18[b]	−19	2.09_{eq}, 2.38_{ax}		
T-3$_T$	−6[b]	−6	2.01_{eq}, 2.04_{ax}		
I-1$_S$	−73[a]	−78	2.03	−67	2.12
I-2$_S$	−52[a]	−49	2.07	−54	2.14
I-2$_T$	−33[a]	−45	2.04	−20	2.15
I-3$_S$	−19[b]	−20	2.08_{eq}, 2.36_{ax}		
I-3$_T$	−18[b]	−19	2.05_{eq}, 2.05_{ax}		
O-1$_{S'}$	−83[a]	−90	1.98	−75	2.08
O-2$_{T'}$	−55[b]	−58	2.06		
O-2$_{S'}$	−63[c]			−59	2.17
O-3$_{T'}$	−33[a]	−40	2.09	−25	2.19
CrIII-1	−56[a]	−58	2.12	−53	2.23
CrIII-2	−48[a]	−50	2.12	−46	2.23
CrIII-3	−50[a]	−55	2.10	−44	2.21
D$_w$-1$_S$	−66[b]	−70	2.01		
	−82[c]			−77	2.11
D$_w$-2$_{SS}$	−73[a]	−79	2.01	−66	2.04
D$_w$-3$_{SS_\mu}$	−31[d]	−31	1.98, 2.26[e]	+3	2.05, 2.42[e]
D$_w$-3$_{SS}$	−27[a]	−25	1.98	−28	2.05
			2.11[f], 2.06		2.13[f], 2.13
D$_w$-3$_{TS}$	−41[a]	−45	2.02_S	−36	2.08_S
			2.05_T		2.14_T
D$_w$-4$_{SS}$	−12[a]	−30	2.10[f], 2.05	+6	2.11[f], 2.14
D$_w$-4$_{TT}$	−18[a]	−32	2.08	−4	2.11
D$_n$-1$_S$	−64[b]	−68	2.04	−74	2.08
D$_n$-2$_{SS}$	−59[a]	−63	2.00	−47	2.06
D$_n$-3$_{SS_\mu}$	−33[d]	−33	2.01, 2.23[e]		
D$_n$-3$_{SS}$	−59[a]	−61	2.02	−57	2.09
			2.05[f], 2.11		2.11[f], 2.15
D$_n$-3$_{TS}$	−28[a]	−44	2.01_S	−12	2.05_S
			2.05_T		2.18_T
D$_n$-4$_{SS}$	−30[a]	−26	2.03[f], 2.08	−33	2.11[f], 2.14
D$_n$-4$_{TT}$	−34[a]	−48	2.05	−20	2.05

[a] $\Delta E^1 = (\Delta E^1_{\text{DFT-1}} + \Delta E^1_{\text{DFT-2}})/2$.
[b] $\Delta E^1 = 0.94 \times \Delta E^1_{\text{DFT-1}}$.
[c] $\Delta E^1 = 1.07 \times \Delta E^1_{\text{DFT-2}}$.
[d] $\Delta E^1 = \Delta E^1_{\text{DFT-1}}$.
[e] CO *cis* to the Cr–O–Cr bridge.
[f] CO in a bridging position between two chromium atoms.

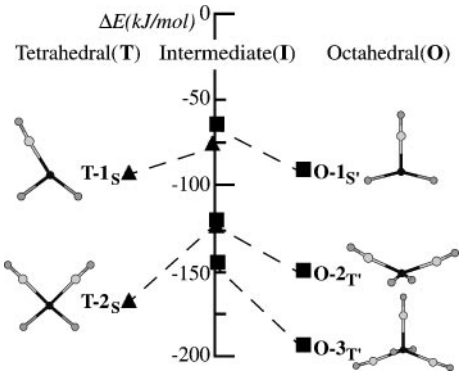

FIG. 5. Structures of the most stable carbonyl complexes formed at the mononuclear Cr(II) cluster models (**T**, **I**, **O**). The structures were optimized using the DFT-1 model, and only the top section of each cluster is shown. The elements are coded on a gray scale according to increasing atom number, C (light gray) < O < Cr (dark gray).

energy" and "coordination energy" are defined as the negative of ΔE[1]. For oligocarbonyls, the binding energy of the complex relative to the naked cluster and isolated CO molecules is obtained by summation of the stepwise adsorption energies. The corresponding overall reaction energy is denoted by ΔE. In the following, the important complexes will be presented for each of the model surface sites.

Mononuclear Cr(II)-A. In Fig. 5, the most stable carbonyl complexes of the mononuclear Cr(II) clusters are presented. They will be referred to by the cluster model and the number of CO ligands, subscripted by either **S** or **T** to specify an idealized coordination geometry about the metal. With two CO ligands coordinated to a divalent chromium center, subscripts **S** and **T** imply square-planar and tetrahedral geometries, respectively. This interpretation is also valid for monocarbonyl complexes, with the understanding that one of the coordination sites is vacant. A prime is added if the ester oxygens are positioned *trans* to each other: **S**′. In the case of three CO molecules, the subscripts are taken to mean square–pyramidal (**S**) and trigonal–bipyramidal (**T**) geometries. The subscripts are primed if the axial positions are occupied by ester oxygens and unprimed if these positions are held by CO. While the square-planar $\mathbf{2_S}$ and square-pyramidal $\mathbf{3_S}$ structures are related in an obvious way, $\mathbf{2_T}$ and $\mathbf{3_T}$ are related to the extent that the tetrahedral $\mathbf{2_T}$ complex may be regarded as a distorted trigonal bipyramid with a vacant equatorial site. This view is useful in connection with the pseudo-octahedral cluster.

The lowest unoccupied molecular orbital (LUMO) of the pseudo-tetrahedral cluster is of b_1 symmetry (see Fig. 1). Accordingly, carbon monoxide coordinates asymmetrically to **T**, i.e., *trans* to an ester oxygen ligand (cf. structure $\mathbf{T\text{-}1_S}$ in Fig. 5). Furthermore, the second carbon monoxide also donates into the LUMO by coordinating in the vacant position *trans* to the other ester oxygen ligand, leaving the dicarbonyl species in a square-planar configuration; $\mathbf{T\text{-}2_S}$. An alternative structure with tetrahedral arrangement about chromium was found to afford only a very low coordination energy of the second carbonyl and is not considered further.

The coordination of a third CO to the $\mathbf{T\text{-}2_S}$ species takes place with the new ligand oriented normal to the coordination plane in $\mathbf{T\text{-}2_S}$ to give a square–pyramidal geometry about chromium. The adsorption energy of the third CO is less than 20 kJ/mol, in concord with a long Cr–C distance of 2.4 Å for the axial CO, i.e., about 0.3 Å longer than the corresponding equatorial distances. The tricarbonyl complex is not considered interesting at or above room temperature.

At the pseudo-octahedral site, repulsion to the ester oxygen ligands enforces symmetrical coordination of the first carbon monoxide (see structure $\mathbf{O\text{-}1_{S'}}$ in Fig. 5). This coordination causes a $1e'' \leftarrow 1a_1'$ excitation of the cluster, thus facilitating donation in the $1a_1'$ orbital. Further coordinations occur in the equatorial plane of the pseudo-octahedral site. The geometry about chromium in the dicarbonyl complex is predicted to be that of a flattened tetrahedron according to DFT-1 (cf. $\mathbf{O\text{-}2_{T'}}$ in Fig. 5), while closer to square–planar using DFT-2. The tricarbonyl complex optimizes to trigonal bipyramidal geometry about chromium (cf. structure $\mathbf{O\text{-}3_{T'}}$ in Fig. 5). The two DFT methods give somewhat different pictures of the stability of this complex (discussed in the following).

Carbonyl complexes at sites of intermediate ∠OCrO bond angles are less stable than those of either tetrahedral or octahedral sites. This may be understood in terms of a reduction in the available coordination space about chromium caused by increasing the ∠OCrO angle from the values realized in the **T** cluster. Alternatively, starting from the **O** cluster, the $1b_1 \leftarrow 2a_1$ excitation that is required to coordinate CO symmetrically is seen from Fig. 1 to get more costly as the ∠OCrO bond angle decreases from 180° into the intermediate range. The implication is that, at a low coverage, the distribution of carbonyl complexes tends to be peaked at either tetrahedral or octahedral sites, or possibly both, even for a distribution of Cr(II) sites that is flat with respect to the ∠OCrO angle. The **I** cluster shows less selectivity with respect to the coordinative geometry about chromium than does the pseudo-tetrahedral site, even though a square-planar geometry is still preferred for the dicarbonyl species. Tricarbonyl species are only weakly bound.

Based on the calibration study in Section 2.2, we form best estimates of stepwise and overall adsorption energies pertaining to each carbonyl complex by averaging the values obtained by DFT-1 and DFT-2 (cf. the second column of Table 3). The numerical discrepancy between the two theoretical models increases with decreasing stepwise adsorption energy and reaches a high for the tricarbonyl complex of the **O** cluster. Whereas DFT-1 predicts the third CO to be

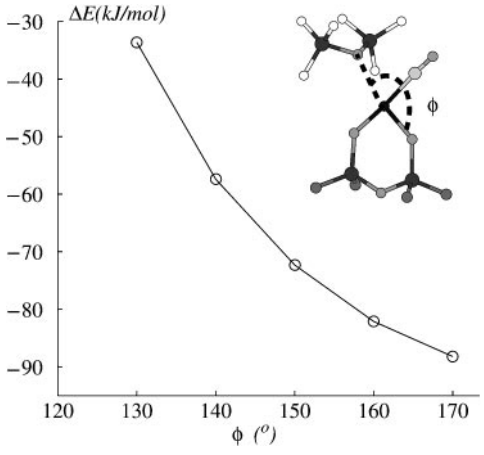

FIG. 6. The energy of CO coordinating to a square–planar mononuclear Cr(II) site (**T**) with a siloxane at a fixed O···Cr distance of 2.42 Å, as a function of the angular orientation of the siloxane donor. The elements are coded on a gray scale according to increasing atom number, H (white) < C < O < Si < Cr (dark gray).

bound by 40 kJ/mol at the octahedral site, DFT-2 recovers less than two-thirds of this value.

Mononuclear Cr(II)-B. Precoordination of oxygen-containing donors is likely to modify and possibly limit the uptake of carbon monoxide at Cr(II) sites. This has been examined for the case of a siloxane donor, $O(SiH_3)_2$, coordinated to the **T** cluster as shown in Fig. 6. In terms of the coordinates defined in the figure, the siloxane optimizes to an O···Cr distance of 2.16 Å, an ∠OCrO angle (ϕ in Fig. 6) of 160°, and a coordination energy of 65 kJ/mol. Thus frozen, the donor reduces the adsorption energy of the first CO by about 20% and leaves the mixed complex about 20 kJ/mol less stable than the corresponding dicarbonyl complex. At the surface, an oxygen donor may face geometric constraints that limit its proximity to chromium, and the strength of the siloxane coordination is found to drop quickly as the O···Cr distance is increased in the interval 2.4–3.0 Å. Taking rigidity at the surface site and the entropy loss during CO adsorption into account, the donor may go from out-competing CO to being easily displaced by a second CO.

In addition to distance constraints, the substrate may also impose constraints on the orientation of the donor. With siloxane fixed at an O···Cr distance of 2.42 Å, the coordinative environment of chromium was transformed from square-planar (with a vacancy) to trigonal-planar by reducing the angle ϕ shown in Fig. 6. In effect, the siloxane moiety was made to pivot on Cr while maintaining a plane of symmetry for the complex. While the coordination energy of the donor was hardly affected by this rotary motion, the reduction in available coordination space leads to a decrease in the affinity toward CO adsorption by 60% at $\phi = 130°$. This reduction is accompanied by an increase in Cr–C distance from 2.06 to 2.13 Å. Furthermore, while the siloxane molecule remains coordinated, chromium shows no affinity toward a second molecule of carbon monoxide.

As far as CO adsorption is concerned, a displaceable oxygen donor is expected to reduce the adsorption energy of CO without affecting the spectroscopic signature of the dicarbonyl complex once it is formed. Hence, displaceable silanol donors are better studied in terms of frequency shifts for the O–H stretching mode due to changes in coordination to chromium. Such changes may occur as a result of decoordination caused by competitive adsorption of CO, or as a result of the metal being oxidized or reduced (cf. Fig. 7).

In an attempt to model these shifts, a difluorosilanol molecule ($SiHF_2OH$) was used to represent the surface silanol functionality. The deprotonation energy of this molecule is calculated to 1428 kJ/mol with DFT-1, in excellent agreement with estimates obtained from computational studies of larger silasesquioxane clusters (20). Moreover, the computed vibrational frequency of the hydroxyl group matches the frequencies observed for isolated hydroxyl species (21). Hence, this model is expected to reproduce the nucleophilic and electrophilic properties of a surface silanol group to a satisfactory extent. The interaction between silanol and the pseudo-tetrahedral monochromium site was studied by means of the cluster models shown in Fig. 7, subject to the following geometric constraints: (i) the $O(SiF_2)_2$ part of the cluster was frozen, and (ii) the SiF_2 part of the difluorosilanol molecule was oriented parallel to the SiOSi moiety at the bottom of the cluster. These constraints effectively reduce the flexibility of both the silanol molecule and the OCrO moiety.

Selected geometry parameters and the shift in OH vibrational frequency of the silanol moiety are presented in Table 4. For the reduced catalyst, we find that a coordination distance of $r(OH\cdots Cr) = 3.8$ Å corresponds to the observed frequency shift of $-42\,cm^{-1}$, assigned to hydroxyls coordinating to reduced chromium surface species by Nishimura and Thomas (21). In their experiment, this peak disappeared completely after subjecting the sample to oxygen at room temperature. In return, a broad absorption band appeared at 3590 cm^{-1}, subsequently assigned to silanols that are hydrogen-bonded to oxo moieties at hexavalent chromium species. The red shift of 157 cm^{-1} is

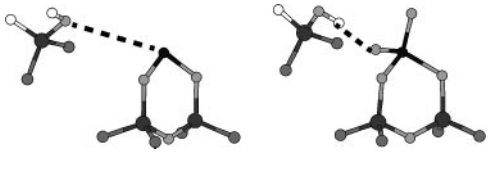

FIG. 7. Models of a difluorosilanol molecule coordinating to a pseudo-tetrahedral cluster with chromium in the divalent (left) (**T**) or hexavalent (right) state (**T**$(oxo)_2$). The elements are coded on a gray scale according to increasing atom number, H (white) < O < F < Si < Cr (dark gray).

TABLE 4

Geometry Parameters, Change in Energy (ΔE) and Shift in OH Stretching Frequency ($\Delta\omega_{OH}$) of Difluorosilanol Coordinating to the Reduced and Oxidized T Cluster

	r(HO···Cr) (Å)	r(OH···OCr) (Å)	ΔE (kJ/mol)	$\Delta\omega_{OH}$ (cm^{-1})
Cr(II)	2.37		−32	−133
	3.04		−11	−63
	3.80		−5	−42
	4.41		−3	−32
Cr(VI)		1.79	−10	−210
		1.95	−15	−158

reproduced in our models at OH···OCr distances just below 2 Å (cf. Table 4). In both cases, the observed frequency shifts suggest that the silanol moieties are facing geometric constraints that limit their proximity to chromium to about 4 Å as given in terms of the O···Cr distance. The coordination energy is about 5 kJ/mol in the reduced case and 15 kJ/mol in the fully oxidized case.

Coordination of one equivalent of CO to the silanol-coordinated Cr(II) is facile and leads to shifts in OH frequency of only a few wave numbers. The adsorption energy of CO is reduced by a couple of kilojoules per mole compared to that of **T-1$_S$**. Upon coordination of a second carbonyl, the weakly bound OH group is easily displaced, effectively decreasing the coordination energy of the second CO by 3–4 kJ/mol and otherwise leaving the dicarbonyl complex as if prepared at a naked Cr(II) site.

Mononuclear Cr(III). The **CrIII** cluster adsorbs the first CO molecule at 46° off the C_3 symmetry axis (see Fig. 8) in agreement with the shape of its lowest unoccupied orbitals (2e in Fig. 3). The first adsorption energy is estimated to 56 kJ/mol, i.e., considerably lower than that found for monocarbonyl Cr(II) complexes. This appears surprising at first, given the donating nature of the bond. However, the three bridges between Cr and the silica structure make the three half-filled metal-dominated orbitals polarize into the open hemisphere. As a consequence, donation into empty d orbitals is accompanied by proximity and thus repulsion, to occupied Cr 3d orbitals. This effectively limits the adsorbate from taking full advantage from the accepting ability of chromium, and the Cr–C bond length remains significantly longer than that at the **T** cluster (see Table 3).

Adsorption of additional CO takes place with only a very modest decrease in binding energy until the tricarbonyl complex is formed. This structure has C_{3v} symmetry, with each CO positioned *trans* to an ester oxygen. The adsorption energies of each of the three CO molecules are then obtained as 56, 48, and 50 kJ/mol, using average energies. Again the discrepancy between the two DFT models increases with CO load to 12 kJ/mol in the case of the third binding energy.

Dinuclear Cr(II). The most stable carbonyl complexes at the **D$_w$** site are presented in Fig. 9 as obtained with DFT-1. To distinguish the structures, the shorthand developed for the mononuclear Cr(II) case is extended to describe the geometry about each of the two chromium atoms. The first subscript applies to the Cr holding the most CO molecules, while a bridging CO is indicated by the subscript μ.

The two computational models disagree with respect to the ground state of the dinuclear clusters and to some extent also to the structure of the corresponding monocarbonyl complexes. According to DFT-1, there are elements of metal–metal bonding in the dinuclear clusters (see molecular orbital $2a_1$ in Fig. 2), giving a Cr–Cr distance of 3.08 Å and a fairly narrow ∠CrOCr angle of 120°. DFT-2 emphasizes the stabilizing exchange interaction within the Cr 3d shell more strongly than does DFT-1, as is evident from the longer Cr–Cr distance of 3.40 Å and an open ∠CrOCr

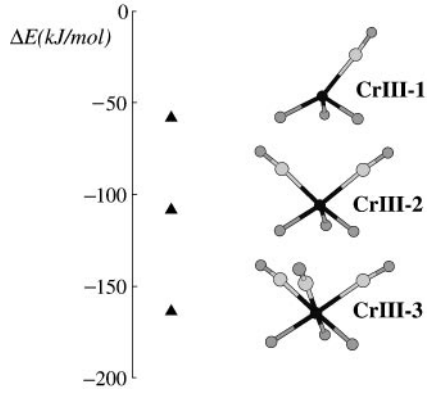

FIG. 8. Structures of the carbonyl complexes formed at the **CrIII** cluster model as obtained with DFT-1. The elements are coded on a gray scale according to increasing atom number, C (light gray) < O < Cr (dark gray).

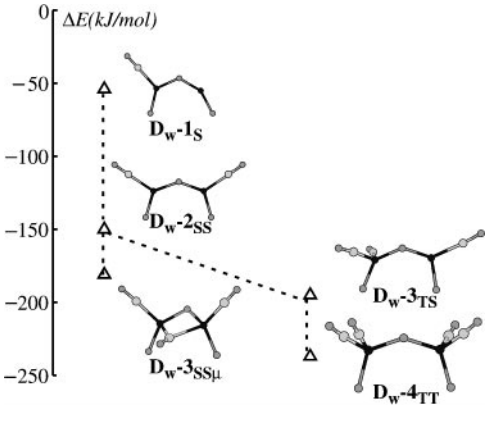

FIG. 9. Structures of the carbonyl complexes formed at the dinuclear chromium cluster model (**D$_w$**), as obtained with the DFT-1 model. The elements are coded on a gray scale according to increasing atom number, C (light gray) < O < Cr (dark gray).

angle of 140°. Moreover, as the $2b_2$ orbital stabilizes and $2a_1$ and $2b_1$ become more nonbonding with the change in geometry, the ground-state electron configuration of the naked clusters as obtained by DFT-2 differs by a single-electron excitation ($2b_2 \leftarrow 3b_1$) from that of DFT-1.

In this situation, we form improved adsorption energies by the scaling procedure developed in the calibration studies. The coordination energies of the first two terminal CO (see structures **D_w-1$_S$** and **D_w-2$_{SS}$** in Fig. 9) become 66 and 74 kJ/mol with DFT-1, and 82 and 71 kJ/mol with DFT-2. For the dicarbonyl as well as higher terminal carbonyls, the two DFT methods agree with respect to both geometric and electronic structures, and average energies are again available (see Table 3).

A second discrepancy between DFT-1 and DFT-2 is encountered when considering CO bridging between the metal atoms. A stable bridging structure is obtained only by means of DFT-1 (see **D_w-3$_{SS\mu}$** in Fig. 9). Since our procedure of scaling the adsorption energy is based on data for terminally coordinated CO, it is not applicable here, and the coordination energy of CO in the bridging position is simply taken as computed by DFT-1. Admittedly, the resulting adsorption energies carry substantial uncertainty.

The main difference between $\mathbf{D_w}$ and the less flexible $\mathbf{D_n}$ cluster becomes apparent when comparing the stabilities of corresponding pairs of **D-2$_{SS}$** and **D-3$_{SS}$** complexes. The constrained geometry of **D_n-2$_{SS}$** makes for facile adsorption of a third terminal CO molecule. Conversely, the open dinuclear cluster supports a more stable dicarbonyl complex, while showing less affinity for further carbonylation. When a third CO is added terminally, this is to form a **D_w-3$_{TS}$** structure, with one metal atom in a tetrahedral environment and the other with trigonally oriented ligands (cf. Fig. 9).

3.2. *Adsorption as a Function of CO Pressure*

For a chromium carbonyl species to be formed in significant amounts and thus become observable in IR spectra recorded at ambient pressure, the adsorption enthalpy must be sufficiently negative to make up for the loss of entropy. The relative concentration of two consecutive carbonyl species at a particular surface site may be expressed in terms of the partial pressure of CO and the reaction enthalpy and entropy of Eq. [1], as $\theta_m/\theta_{m-1} = \exp(\Delta S^1/R) \times \exp(-\Delta H^1/RT) \times p_{CO}$. θ_0 denotes the equilibrium concentration of vacant sites of the kind in question. The entropy term depends only weakly on the specific choice of site and adsorption steps, and from DFT-2 calculations of a monocarbonyl complex at the **T** cluster, we find $\Delta S = -15R$, corresponding to a free-energy contribution of $-T\Delta S \sim 37$ kJ/mol at room temperature. In the following, we will assume the adsorbent to furnish detectable amounts of pseudo-tetrahedral mononuclear Cr(II), mononuclear Cr(III), and dinuclear Cr(II) sites.

Even at a very low pressure of CO, adsorption equilibria with enthalpy changes below −70 kJ/mol will be shifted toward the adsorbed complexes. This class includes dicarbonyl species at the pseudo-tetrahedral Cr(II) cluster and monocarbonyl species at Cr(II)-B sites. Consequently, monocarbonyl species at the Cr(II)-A site are probably not observed. However, the concentration of **T-2** species may display pressure dependence, as the presence of a displaceable silanol group renders the second CO coordination energy slightly less facile. Furthermore, since the adsorption energy associated with Cr(II)-B sites gets less favorable the closer and more symmetrically the oxygen donor is coordinated to the metal, one may expect a gradually increasing concentration of **T-1**-like complexes as the CO pressure is increased. If present, Cr(II) sites with a wider-than-tetrahedral ∠OCrO angle support the formation of monocarbonyl species even at a very low CO pressure, here represented by **I-1$_S$** and **O-1$_S$**. Contrary to the pseudo-tetrahedral case, the adsorption equilibria shift toward dicarbonyl complexes only as the CO pressure is increased.

The two DFT models disagree with respect to the stability of the monocarbonyl dinuclear complex, yet agree on other features of the dinuclear sites. The coordination of CO to geometrically flexible sites ($\mathbf{D_w}$) precede those to more strained sites ($\mathbf{D_n}$) and show somewhat different pressure dependency. At the $\mathbf{D_w}$ dinuclear site, the carbonyl equilibrium is expected to shift directly toward the **D_w-2$_{SS}$** dicarbonyl complex, with one CO bound terminally to each chromium center. Subsequent coordinations are predicted to be less facile and thus to occur at a later stage. On the other hand, at the narrow-bite $\mathbf{D_n}$ cluster, the equilibrium is probably shifted toward the **D_n-3$_{SS}$** complex in the same pressure range that is supporting the dicarbonyl complex at $\mathbf{D_w}$.

Carbonyl complexes at **CrIII** sites constitute the next class, with enthalpy changes in the region of −60 to −50 kJ/mol. The stepwise adsorption energies are almost constant up to three coordinated CO molecules, and we expect the monocarbonyl complex to be observable only in a narrow pressure range, before shifting the equilibrium toward the tricarbonyl complex, **CrIII-3**. Beyond this stage, less facile coordinations to the dinuclear sites may dominate the uptake of CO. For instance, the coordination of a third CO to **D_w-2$_{SS}$** may give rise to three different complexes, with associated changes in enthalpy between −41 to −27 kJ/mol.

3.3. *Macro Assignment of the IR Vibrational Spectrum*

Of the systems studied here, the mononuclear tetrahedral Cr(II) site supports the highest coordination energies and thus constitutes a natural starting point for presenting carbonyl vibrational frequencies. The two theoretical models lead to quite disparate results for the monocarbonyl

complex, with harmonic frequencies of 2064 cm^{-1} (DFT-1) and 2214 cm^{-1} (DFT-2). The discrepancy remains if first-order shifts are considered, since DFT-1 predicts a red shift of -52 cm^{-1} upon coordination while a blue shift of 7 cm^{-1} is predicted by DFT-2. These shifts are matched by the predicted changes in the bond length of carbon monoxide upon coordination, which are +0.5 pm and −0.3 pm for DFT-1 and DFT-2, respectively.

Despite the differences noted for the monocarbonyl complex, DFT-1 and DFT-2 give fairly consistent pictures of the process of adding a second carbonyl to this site. Both methods predict the C–O bond to contract slightly, with shifts to higher frequency of both of the CO stretching modes, if only minutely in the case of the antisymmetric B_1. The symmetric mode is shifted by 28 cm^{-1} (DFT-1) and 19 cm^{-1} (DFT-2). Hence, the splitting of the symmetric A_1 and asymmetric B_1 vibration of the **T-2** dicarbonyl complex comes out as 24 and 18 cm^{-1} with DFT-1 and DFT-2, respectively. In this case, the agreement between the methods is satisfactory, suggesting that the problems observed for the monocarbonyl complex may be solved by evoking a more relevant reference state than gas-phase carbon monoxide.

In Fig. 10, the carbonyl vibrational frequencies of the complexes expected to be observable are shown as computed with both DFT-1 and DFT-2, using the frequency of the asymmetric CO stretching mode of the **T-2** complex as a reference. The two computational methods are seen to agree on the following partitioning of the spectrum: (i) a low-frequency region, at 30–60 cm^{-1} below the asymmetric **T-2** frequency; (ii) an intermediate region, from 0 to 30 cm^{-1} above this frequency; and (iii) a high-frequency region, more than 30 cm^{-1} above the reference frequency. These frequency regions are characteristic for different adsorption sites, with dinuclear sites making up the low-frequency part. CO adsorbed to mononuclear Cr(II) sites of different local geometries constitutes the intermediate region, while CO on mononuclear Cr(III) sites makes up the high-frequency region.

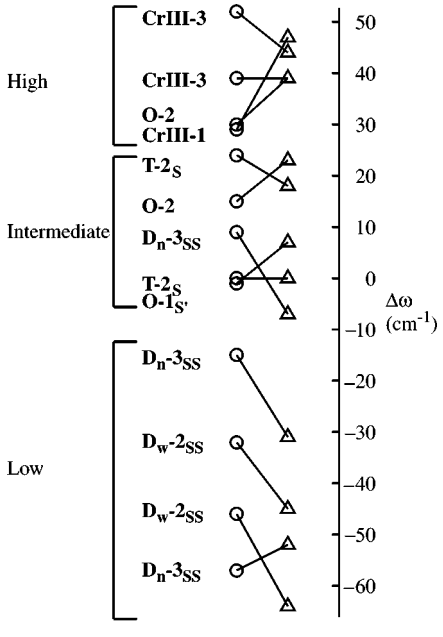

FIG. 10. Shifts in vibrational frequencies of carbonyl complexes predicted to be observable (cf. the text), relative to the asymmetric **T-2** mode, as computed using DFT-1 (◯) and DFT-2 (△).

The correlation between frequency regions and adsorption sites seemingly breaks down in a couple of instances; e.g., the symmetric mode of the **O-2** dicarbonyl complex appears in the lower part of the high-frequency region. However, due to the relative orientation of the CO molecules, the symmetric A_1 vibration of the **O-2** dicarbonyl complex becomes IR inactive and will not show up in the spectrum. Conversely, the antisymmetric B_2 vibration receives a boost in intensity, and the **O-2** dicarbonyl complex is expected to give rise to only one peak, possibly overlapping with the symmetric **T-2**(A_1) band. A second deviation from the pattern is made by the tricarbonyl complex at the narrow-bite dinuclear site, $\mathbf{D_n\text{-}3_{SS}}$, to be addressed in the following.

3.4. Micro Assignment of the IR Vibrational Spectrum

In this section, we establish an interpretation of the experimentally observed carbonyl Cr/Silica IR spectra by means of computed stabilities, the shifts in vibrational frequencies, and the IR intensities of model carbonyl–cluster complexes. Because of the significant uncertainties associated with the vibrational frequencies in particular, such an assignment is less than straightforward and has to be made in close comparison to experimental observations. The evolution of the carbonyl Cr/Silica IR spectra with increasing CO pressure has been recorded at room temperature by Ghiotti *et al.* (4) and at 77 K by Zecchina *et al.* (11). These spectra are especially useful for comparison to our computed results, as they facilitate discrimination of carbonyl complexes with respect to stability, at least in a qualitative manner, as well as shifts of vibrational frequencies.

The room-temperature spectra reveal spectroscopic features of the carbonyl complexes at the most acidic of the Cr surface sites. At a low equilibrium pressure of 0.2 Torr, the room-temperature spectrum reveals two bands positioned at 2180 and 2191 cm^{-1}, with an intensity ratio of about 2 : 1 (4). Upon increasing the pressure, the 2180-cm^{-1} band transforms into an increasingly intense band positioned at 2184 cm^{-1} with a shoulder at 2178 cm^{-1}. At a pressure of 40 Torr, the 2178/2191 intensity ratio has decreased to 4 : 3 (4). The bands positioned at 2178, 2184, and 2191 cm^{-1} are commonly termed the room-temperature triplet. At low temperatures, a new triplet of bands appears, positioned at 2045, 2100, and 2120 cm^{-1}, which is referred to as the low-temperature triplet of bands (11).

Based on our computed adsorption energies and vibrational frequencies and the assumption that tetrahedral,

mononuclear Cr(II) species are present in ample amounts, we assign the 2178-cm^{-1} peak to the asymmetric **T-2**(B_1) mode and the 2191-cm^{-1} peak to the symmetric **T-2**(A_1) mode (see Table 6). The computed splitting is too high by 5–11 cm^{-1}, a deviation from the experiment that is compatible with the accuracy of our calculations (19, 18). The more stable monocarbonyl complexes at Cr(II)-B sites are also predicted to be formed at relatively low CO pressure, shifting the low-frequency component of the room-temperature triplet to 2180 cm^{-1}. Moreover, we see the contribution from monocarbonyl Cr(II)-B species as an explanation for the 2 : 1 intensity ratio between the 2180- and 2191-cm^{-1} peaks. Cr(II)-B sites with a displaceable oxygen donor eventually form dicarbonyl complexes and thus show up as **T-2** species in the IR spectrum, in accordance with the observed decrease in the 2178/2191 ratio with increasing CO pressure.

Furthermore, we assign the 2184-cm^{-1} band to monocarbonyl complexes at Cr(II)-B sites that are significantly affected by the presence of a nondisplaceable oxygen donor. This is in agreement with the calculations, which gave a small blue shift of the vibrational frequency and reduced stability of the monocarbonyl complex, compared to that without a siloxane coordinating to chromium. For such species to give rise to a separate peak, we propose a nonuniform distribution with respect to the oxygen donor coordination. Localized nests of hydroxyls, due to the lack of one [SiO_4] building unit, may act as grafting centers for chromic acid. Subsequent dehydroxylation and reduction would give rise to Cr(II)-B sites with a distinct coordination environment (22).

Mononuclear Cr(II) sites that differ with respect to the ∠OCrO angle may add additional structure to the carbonyl IR spectra. The **I-2$_S$** complex contributes to the same bands as the dicarbonyl complex at the tetrahedral site, while the **O-2** complex contributes only in the frequency region associated with the symmetric **T-2**(A_1) vibration. Thus, the presence of such sites causes the intensity of the band associated with the symmetric **T-2**(A_1) vibration to display additional pressure dependence.

New bands at lower frequencies develop in the room-temperature spectra with increasing CO pressure (4, 10). These bands are, however, best seen in the low-temperature spectra (11). The first appears at 2100 cm^{-1}, with a full-width-at-half-maximum (fwhm) close to that of the high-temperature triplet. The first sign of a peak at 2120 cm^{-1} is observed at this early stage, but a full band develops only after a third band is formed at 2045 cm^{-1}, along with a red-shifted shoulder. Furthermore, the 2120- and 2045-cm^{-1} peaks are of comparable intensity, which, moreover, is about two-fifths of that of the 2100-cm^{-1} band. These three bands are referred to as the low-temperature triplet.

With an increase in pressure, the intensities of the 2100- and 2120-cm^{-1} peaks increase and the fwhm's approach three-fourths, and one-half respectively, of that of the high-temperature triplet. The 2045-cm^{-1} band shows only a modest increase in intensity, yet its red-shifted shoulder grows without separating from the initial band. Thus, a very broad band results in 2045–2035 cm^{-1}, with a fwhm about twice that of the high-temperature triplet (11).

According to our computed stability data, CO adsorption at dinuclear sites occurs when the more acidic mononuclear sites reach intermediate saturation, and the dicarbonyl complex at the **D$_w$** site is predicted to be the first structure observable in the IR spectrum. Moreover, this complex is expected to give rise to a single intense peak, computed at 46 and 64 cm^{-1} below the asymmetric **T-2**(B_1) frequency according to DFT-1 and DFT-2, respectively. This fits well with the observation that the first band of the low-temperature triplet is red-shifted by 78 cm^{-1} relative to the 2178-cm^{-1} peak of the high-temperature triplet. Hence, the 2100-cm^{-1} peak is identified as the asymmetric B_1 mode of the **D$_w$-2$_{SS}$** dicarbonyl complex. The significantly less intense symmetric mode is calculated at 14 cm^{-1} (DFT-1) and 19 cm^{-1} (DFT-2) higher frequency. Thus, we assign the 2120-cm^{-1} band to the symmetric **D$_w$-2$_{SS}$** mode.

Given the assignments made thus far, the CO stretching frequencies computed for the remaining dinuclear complexes need to be corrected by −14 cm^{-1} in the case of DFT-2, and by −32 cm^{-1} in the case of DFT-1. Subsequent adsorption of CO is predicted to take place at the **D$_n$** dinuclear cluster model, giving rise to tricarbonyl complexes of **D$_n$-3$_{SS}$** character. The associated IR transitions come as three well-separated peaks, and while the theoretical methods agree on the two highest frequencies, at 32 and 56 cm^{-1} above the 2100-cm^{-1} peak, the two peaks observed in this region, at 2138 and 2158 cm^{-1}, do not display the predicted intensity ratio. Also, they appear at a higher CO pressure than indicated by the stability of the current complex. In the literature, these peaks are assigned to CO physisorbed at dehydroxylated parts of the surface (2138 cm^{-1}) and CO hydrogen bonded to silanols (2158 cm^{-1}).

A third terminal coordination at the **D$_w$** cluster gives rise to the **D$_w$-3$_{TS}$** carbonyl complex. According to Table 5, the spectral properties of this complex are quite similar to those of the **D$_n$-3$_{SS}$** complex just reviewed. Hence, it appears that terminal tricarbonyl complexes are not contributing significantly to the IR spectrum of these systems, and, in particular, that such species are not able to account for the observed evolution of the low-temperature triplet.

A tricarbonyl complex may be formed at a dinuclear site in yet another way, namely, by coordinating the third CO in a bridging position as exemplified by **D$_w$-3$_{SS_\mu}$** and **D$_n$-3$_{SS_\mu}$**. While the computed stabilities of these complexes suggest fairly late population in terms of CO pressure, we recognize that a theoretical description of a bridging CO molecule may be more demanding than one of a terminally

TABLE 5

Vibrational Frequencies, IR Intensities, and Carbon–Oxygen Bond Lengths of Carbonyl Complexes at Cluster Models of Cr/Silica

	DFT-1			DFT-2		
	rC–O(Å)	$\omega_{as}{}^a$ (cm^{-1}), I(D^2 Å^2 amu)	$\omega_s{}^a$ (cm^{-1}), I(D^2 Å^2 amu)	rC–O(Å)	$\omega_{as}{}^a$ (cm^{-1}), I(D^2 Å^2 amu)	$\omega_s{}^a$ (cm^{-1}), I(D^2 Å^2 amu)
CO(g)	1.141		2113, 2	1.129		2207, 2
T-1$_S$	1.146		2064, 13	1.126		2214, 13
T-2$_S$	1.142	2068, 12	2092, 11	1.125	2215, 11	2233, 9
I-1$_S$	1.146		2057, 13	1.127		2212, 13
I-2$_S$	1.143	2073, 11	2090, 9	1.126	2212, 17	2229, 10
O-1$_{S'}$	1.144		2067, 8	1.126		2222, 9
O-2$_{T'}$	1.142	2083, 16	2098, 1			
O-2$_{S'}$				1.124	2238, 13	2254, 0
O-3$_{T'}$	1.142	2078, 16	2081, 9	1.126	2212, 15	2219, 8
			2103, 1			2233, 1
CrIII-1	1.140		2097, 11	1.122		2262, 5
CrIII-2	1.139	2103, 8	2114, 10	1.123	2256, 5	2261, 5
CrIII-3	1.139	2107, 14	2120, 9	1.123	2254, 10	2259, 5
D$_w$-1$_S$	1.149		2017, 21	1.130		2177, 24
D$_w$-2$_{SS}$	1.148	2022, 39	2036, 9	1.132	2151, 40	2170, 12
D$_w$-3$_{SS_\mu}$	1.152[b]		2004, 9	1.129[b]		
	1.148	2031, 25	2049, 10	1.130		
D$_w$-3$_{TS}$	1.149$_S$	2013, 29		1.133$_S$	2152, 27	
	1.144$_T$	2058, 19	2075, 9	1.126$_T$	2205, 18	2223, 3
D$_n$-1$_S$	1.148		2045, 19	1.130		2182, 19
D$_n$-2$_{SS}$	1.152	1997, 27	2021, 22	1.131	2161, 48	2179, 6
D$_n$-3$_{SS_\mu}$	1.156		1975, 9	—		
	1.150	2020, 24	2038, 15	—		
D$_n$-3$_{SS}$	1.150		2011, 26	1.131		2163, 29
	1.146[c]	2077, 18	2053, 13	1.129[c]	2208, 12	2184, 15
	1.142			1.127		
D$_n$-3$_{TS}$	1.151$_S$	2018, 30		1.132$_S$		
	1.148$_T$	2025, 21	2050, 13	1.130$_T$		
D$_n$-4$_{SS}$	1.148[c]	2025, 2	2037, 13	1.130		
	1.144	2046, 40	2074, 9	1.128[c]		
D$_n$-4$_{TT}$	1.147	2034, 40	2028, 0	1.130		
		2025, 32	2062, 5			

[a] Subscripts *s* and *as* denote symmetric and antisymmetric CO stretching modes, respectively.
[b] CO in a bridging position between two chromium atoms.
[c] CO *cis* to the Cr–O–Cr bridge.

coordinated CO. To clarify this point, the **D$_w$-2$_{SS}$** and **D$_w$-3$_{SS_\mu}$** complexes were reexamined using the larger Gaussian-type basis sets described in the Appendix. Following reoptimization of geometries and calculation of harmonic vibrational frequencies through analytical evaluation of the full Hessian, we find the stability of the bridged tricarbonyl complex to be improved by 7 kJ/mol. More importantly, compared to the asymmetric stretching mode involving the two terminal CO ligands at this complex, the red shift of the frequency pertaining to the bridging CO increases from 26 to 53 cm^{-1}. Undertaking the same kind of reexamination of the analogous structures at **D$_n$**, the corresponding red shift increases from 45 to 80 cm^{-1}, albeit without changing the stability of the bridging complex appreciably. Hence, the bridging tricarbonyl complex is less stable at a narrow-bite than at a wide-bite dinuclear site, yet produces a larger red shift in the IR spectrum once formed.

The three CO stretching modes of **D$_w$-3$_{SS_\mu}$** give rise to peaks in the IR spectrum with an intensity ratio of 2 : 5 : 2. For comparison, at a CO pressure at which the 2120 cm^{-1} has developed into a full peak, this is the intensity pattern observed between the bands at 2120, 2100, and 2045 cm^{-1}. The frequencies of the two stretching modes involving terminal CO's are split by 18 cm^{-1} (21 cm^{-1} using the larger basis sets), and, invoking a red shift of 9 cm^{-1}, these are seen to match those of the **D$_w$-2$_{SS}$** dicarbonyl species, already assigned to the 2100- and 2120-cm^{-1} bands. Based on the improved estimates of the frequency of the third, red-shifted mode that mainly involves stretching of the bridging CO, we tentatively assign the 2045-cm^{-1} band to this mode. The

TABLE 6

Theoretical Assignment of Carbonyl–Cr/Silica IR Spectra

IR band (cm^{-1})	CO Pressure		
	Low	Intermediate	High
2212			**CrIII-3**(A_1)
2200			**CrIII-3**(E)
2191	**T-2**(A_1)	**O-2**(B_2)	
2184		**Cr(II)**-B-**1**	
2178	**T-2**(B_1)		
2120		$\mathbf{D_w}$-$\mathbf{2_{SS}}$(A_1)	$\mathbf{D_w}$-$\mathbf{3_{SS_\mu}}$(A')[a]
2100		$\mathbf{D_w}$-$\mathbf{2_{SS}}$(B_1)	$\mathbf{D_w}$-$\mathbf{3_{SS_\mu}}$(A'')[a]
2045			$\mathbf{D_w}$-$\mathbf{3_{SS_\mu}}$(A')[a]

[a] Only observable at low temperatures due to unfavorable loss of entropy.

observed broadening of the band toward lower frequencies with increasing CO pressure is consistent with the formation of bridged tricarbonyl species of lower stability, such as modeled by $\mathbf{D_n}$-$\mathbf{3_{SS_\mu}}$. The entropy loss upon adsorption is found to be 40% higher when a CO molecule is coordinating in a bridging position as compared to in a terminal position. This implies that the infrared frequency associated with a bridging CO, at 2035–2045 cm^{-1}, is observable only in spectra recorded at low temperatures.

Returning to the room-temperature spectra, at a high CO pressure of 1 atm, Kohler and Ekerdt (10) observed two low-intensity bands at 2200 and 2212 cm^{-1}, in addition to the room-temperature triplet. The 2212-cm^{-1} band carries about half the intensity of the band at 2200 cm^{-1}. Of the cluster models considered in this work, only **CrIII** supports carbonyl complexes with vibrational frequencies in this region. Furthermore, the Cr(III) site is predicted to reach saturation with respect to CO uptake over a fairly narrow pressure region, as the adsorption energy is very similar among the first three CO ligands. Relative to the **T-2**(B_1) mode, the theoretical methods agree upon a 39-cm^{-1} blue shift of the E mode of the tricarbonyl complex. Furthermore, the symmetric A_1 mode is blue-shifted by 5–13 cm^{-1}, carrying half the intensity of the doubly degenerate E mode. These features are in fair correspondence with the properties observed for the 2200- and 2212-cm^{-1} bands, which are assigned accordingly (cf. Table 6). Implicit in this assignation is the recognition that our methods may overestimate the intermolecular shift between **CrIII-3**(E) and **T-2**(B_1) frequencies by as much as 17 cm^{-1}.

4. DISCUSSION

At this point, it is useful to contrast our assignment of the carbonyl IR spectrum as it appears in Table 6 to those of other workers. Kohler and Ekerdt (10) evaluated the ratios of integrated IR intensities of the peaks observed at 2178, 2184, 2191, and 2212 cm^{-1} during isothermal evacuation at room temperature. The 2191/2184 intensity ratio was found to increase upon evacuation, reaching a value of ~0.75 at the end of the observation period. The initial increase of this ratio is in line with our interpretation of the spectra, as desorption of CO is expected to occur more readily at Cr(II)-B sites with a closely coordinated oxygen donor than at Cr(II)-A sites. Furthermore, our assignment of the band at 2184 cm^{-1} to a monocarbonyl Cr(II) species agrees with Kohler and Ekerdt and differs from other suggestions, such as those involving *mer*-$(CO)_3$Cr(II) species (4) or terminal carbonyls at dinuclear sites (5).

The 2191/2178 intensity ratio initially undergoes a modest decrease before leveling off at a constant value. Nishimura and Thomas observed an inverse correlation between the decreasing intensity of the 2191-cm^{-1} peak and the appearance of a peak at 3705 cm^{-1}, assigned to displaceable hydroxyl groups interacting with a Cr(II) site upon evacuation of CO. This behavior is accounted for by desorption of one equivalent of CO at Cr(II)-B sites with a coordinating silanol, following the proposal by Nishimura and Thomas (21). The close-to-constant 2191/2178 intensity ratio is readily understood as these bands correspond to the same dicarbonyl species, again in agreement with the interpretation made by Kohler and Ekerdt.

Based on the computed stability data, the 2212/2190 intensity ratio is expected to decrease with reduced CO pressure, due to desorption of CO from Cr(III) sites. While this fits the evolution of these peaks in the IR spectra recorded at 77 K by Zecchina *et al.* (11), Kohler and Ekerdt observed a close-to-constant intensity ratio. According to the DFT-2 calculations, even monocarbonyl and dicarbonyl complexes at Cr(III) surface sites contribute to the 2212 peak. In this scenario, the intensity of the peak would be sustained through the equilibrium shift from tricarbonyl to dicarbonyl and further to monocarbonyl complexes, and the intensity ratio would depend on whether it was observed at equilibrium or after evacuation for a limited period of time.

Our assignment of the peak at 2212 cm^{-1} to Cr(III) carbonyl complexes leaves us with a discrepancy toward the interpretation of Kohler and Ekerdt, who proposed the 2178-, 2191-, and 2212-cm^{-1} peaks to arise from the same *mer*-$(CO)_3$Cr(II) structure of C_{2v} symmetry. In fact, both Kohler and Ekerdt (10) and Ghiotti *et al.* (4) propose the formation of Cr(II) tricarbonyl species at low-to-intermediate CO pressure. We find that freely relaxed, the *mer*-$(CO)_3Cr(II)(OSiF_3)_2$ cluster model adopts D_{3h} geometry. In order for the A_1' vibration to obtain intensity, the structure must distort into C_{2v} symmetry, possibly caused by a weak interaction with the surface. Fixing the ∠CCrC angle at 110° causes the E mode to split into $(A_1)_2$ and B_2. Relative to the more intense B_2 mode, the A_1 modes are predicted at 5 and 26 cm^{-1} higher frequency and with intensities of 0.54 and 0.08, respectively. These spectroscopic properties are in fair agreement with those assigned to the tricarbonyl species proposed by Kohler and Ekerdt.

However, according to the free energy of complexation, the third CO is barely bound at room temperature and may form only at an elevated CO pressure. Restricting the CO molecules further to occupy only the (upper) hemisphere, as suggested by Kohler and Ekerdt (10), causes reordering of the $(A_1)_2$ and B_2 modes. While this leaves the most intense B_2 band blue shifted relative to $(A_1)_2$ as proposed by Ghiotti *et al.* (4), the third CO turns out unbound, at a free energy of complexation of +26 kJ/mol at room temperature.

Turning to the low-temperature triplet of bands, Rebenstorf assigned all three bands to CO bridging at dinuclear sites (5). This was based on the known fact that the stretching frequency of CO bound in a bridging position is red-shifted compared to the frequencies associated with terminal CO. Kohler and Ekerdt found that the 2100/2190 intensity ratio increased with the chromium loading (10). Since the dinuclear-to-mononuclear ratio is known to increase with Cr loading on pyrogenic silica (6), assignation of the 2100-cm^{-1} band to CO coordinated to dinuclear sites seems reasonable. However, the integrated intensity of peaks corresponding to carbonyls in the bridging mode are known to be distinctly lower than those of terminal coordinations. The high intensity of the 2100- and 2120-cm^{-1} peaks observed in low-temperature spectra renders assignation of these bands to terminal coordinations more likely. Thus, these observations support our assignation of the low-temperature triplet.

5. CONCLUSION

Cluster models and density functional theory have been used to explore the structure, stability, and vibrational properties of carbonyls formed at low-valent chromium bound to silica. The models have limitations in the assumptions made in their construction, such as the neglect of the extended silica structure, as well as the accuracy with which we are able to describe the electronic structure of the model species. However, by comparing the computed spectral and thermodynamical properties for the various surface sites with observations, we are able to provide a consistent interpretation of the infrared spectra of the reduced Cr/silica as exposed to carbon monoxide, at different values for the CO pressure and the temperature.

The pseudo-tetrahedral, mononuclear Cr(II) site is found to adsorb two molecules of CO even at a low pressure. Together with monocarbonyl species formed at a similar site with an indisplaceable oxygen donor, the properties of these complexes are consistent with the room-temperature triplet found in experimental IR spectra. The evolution with CO pressure of the so-called low-temperature triplet in these spectra is consistent with our results for terminal dicarbonyl species and tricarbonyl species with one bridging CO, at dinuclear, divalent chromium sites. Finally, tricarbonyl complexes formed at mononuclear, trivalent chromium sites give rise to two absorptions in the infrared regime at high frequencies.

A consequence of the proposed interpretation of the observed infrared spectrum is that dichromium species exist in appreciable amounts on the reduced Cr/silica system, both when pyrogenic and sol–gel silica is used as support. Furthermore, Cr(II)-B sites appear to be present in appreciable amounts, most likely exceeding the concentration of Cr(II)-A.

APPENDIX

Quantum Chemical Models

This study was conducted in terms of two different density functional theory (DFT) models, denoted as DFT-1 and DFT-2 respectively. In both cases, basis sets of at least triple-ζ quality were used on all atoms, and closed- and open-shell systems were described within spin-restricted and -unrestricted formalisms, respectively.

In DFT-1, which uses a pure generalized gradient-corrected DFT method, electron correlation is provided by the functional fitted to the Ceperly–Alder solution of the uniform electron gas by Vosko *et al.* (23) together with the nonlocal correction by Perdew (24). The exchange potential consists of the Slater functional augmented by Becke's 1988 gradient correction (25). Molecular orbitals were formed in atom-centered primitive Slater-type basis sets supplied with the computer code used, Amsterdam Density Functional (26, 27), and detailed in Ref. (28). Polarization functions were added to all atoms except chromium. Atomic cores, defined as the K shell for first-row elements and K and L shells for second- and third-row elements, were kept frozen. Molecular geometries were converged to a gradient below 0.001 E_H/Å. The numerical integration parameter was set to 4.5, albeit adjusted to 6.0 in frequency calculations, which were done by two-point numerical differentiation in the C–O bond lengths. To check for possible coupling to other internal degrees of freedom, full force-constant matrices were computed for the **T-2** and **O-1** complexes. The **O-1** and symmetric **T-2** CO frequencies remained unchanged within 1 cm^{-1}, whereas the asymmetric CO stretching frequency in **T-2** dropped by 6 cm^{-1} compared to the value obtained from the truncated force field. The infrared intensities of all relevant modes were found to increase as the force field was made more complete, albeit with small changes in relative intensities between modes associated with the same complex. These changes are within the margins used when discussing shifts in vibrational frequencies and intensities. As detailed in Section 3.4 for a dinuclear site, the vibrational frequency associated with a bridging CO ligand is notably more affected by truncations in the force field.

DFT-2 uses the B3LYP hybrid density functional (29) as implemented (30) in the Gaussian-98 set of programs (31).

In this functional, exchange effects are modeled by both explicit Hartree–Fock exchange and effective local and nonlocal density functionals. Molecular orbitals were formed in atom-centered Gaussian-type bases of triple-ζ quality as extended by diffuse and polarization functions and detailed in Ref. (15). The electron density was evaluated at a grid with 75 radial shells per atom and 302 angular points per shell. Molecular geometries were converged to a gradient below 0.00045 E_H/Bohr. Vibrational frequencies and infrared intensities were obtained in the harmonic approximation by analytical evaluation of the Hessian. The algorithm applied when evaluating the Hessian is valid at stationary points only, and may in principle lead to problems when used in conjunction with frozen internal coordinates, as was the case for two of our models (**O** and $\mathbf{D_w}$). However, judging from the preceding paragraph, the frozen coordinates couple very weakly to the CO stretching modes, and hence only minute errors are expected to result from nonvanishing gradient elements. This view is corroborated by results from the numerical evaluation of force constants in the dicarbonyl **O-2** complex. In this test calculation, the Hessian was computed based on gradient information from geometries in which only freely optimized atoms were displaced. The resulting CO vibrational frequencies were within 1 cm^{-1} of those obtained from analytical evaluation of the Hessian.

A limited number of *ab initio* coupled-cluster calculations were carried out to obtain precise CO adsorption energies. These calculations were performed in geometries as optimized at the DFT-2 level of theory, and include single and double excitations as well as a perturbative estimate of the energy contribution from triple excitations (CCSD(T)). To make the calculations feasible, the basis sets of the main group elements were replaced by double-ζ basis sets (cc-pVDZ) (32–34), albeit augmented by the diffuse s and p functions of the aug-cc-pVDZ sets. The computed correlation effects were extrapolated toward a complete correlation treatment according to the parameterized configuration–interaction scheme (PCI-X) proposed by Siegbahn *et al.* (35), with $X = 83\%$ (36).

ACKNOWLEDGMENTS

We are grateful to the Research Council of Norway for financial support, and for a grant of computing time (Programme for Supercomputing).

REFERENCES

1. Niemantsverdriet, J. W., "Spectroscopy in Catalysis." VCH, Weinheim, 1995.
2. Davydov, A. A., "Infrared Spectroscopy of Adsorbed Species on the Surface of Transition Metal Oxides." Wiley, Chichester, 1990.
3. Weckhuysen, B. M., and Schoonheydt, R. A., *Catal. Today* **51**, 215 (1999).
4. Ghiotti, G., Garrone, E., and Zecchina, A., *J. Mol. Catal.* **46**, 61 (1988).
5. Rebenstorf, B., *J. Polym. Sci., Part A: Pol. Chem.* **29**, 1949 (1991).
6. Weckhuysen, B. M., Wachs, I. E., and Schoonheydt, R. A., *Chem. Rev.* **96**, 3327 (1996).
7. McDaniel, M. P., *Adv. Catal.* **33**, 47 (1985).
8. Fubini, B., Ghiotti, G., Stradella, L., Garrone, E., and Morterra, C., *J. Catal.* **66**, 200 (1980).
9. Weckhuysen, B. M., De Ridder, L. M., and Schoonheydt, R. A., *J. Phys. Chem.* **97**, 4756 (1993).
10. Kohler, S. D., and Ekerdt, J. G., *J. Phys. Chem.* **98**, 4336 (1994).
11. Zecchina, A., Spoto, G., Ghiotti, G., and Garrone, E., *J. Mol. Catal.* **86**, 423 (1994).
12. Zielinski, P. A., Szymura, J. A., and Lana, I. G. D., *Catal. Lett.* **13**, 331 (1992).
13. Zielinski, P., and Lana, I. G. D., *J. Catal.* **137**, 368 (1992).
14. Espelid, Ø., Børve, K. J., and Jensen, V. R., *J. Phys. Chem. A* **102**, 10,414 (1998).
15. Espelid, Ø., and Børve, K. J., *Catal. Lett.* **75**, 49 (2001).
16. Huber, K. P., and Herzberg, G. P., "Constants of Diatomic Molecules." Van Nostrand Reinhold, New York, 1979.
17. Adamo, C., and Lelj, F., *J. Chem. Phys.* **103**, 10,605 (1995).
18. Spears, K. G., *J. Phys. Chem. A* **101**, 6237 (1997).
19. Jonas, V., and Thiel, W., *Organometallics* **17**, 353 (1998).
20. Civalleri, B., Garrone, E., and Ugliengo, P., *Chem. Phys. Lett.* **294**, 103 (1998).
21. Nishimura, M., and Thomas, J. M., *Catal. Lett.* **21**, 149 (1993).
22. Spoto, G., Bordiga, S., Garrone, E., Ghiotti, G., and Zecchina, A., *J. Mol. Catal.* **74**, 175 (1992).
23. Vosko, S. H., Wilk, L., and Nusair, M., *Can. J. Phys.* **58**, 1200 (1980).
24. Perdew, J. P., *Phys. Rev. B* **33**, 8822 (1986).
25. Becke, A. D., *Phys. Rev. A* **38**, 3098 (1988).
26. Guerra, C. F., Snijders, J. G., te Velde, G., and Baerends, E. J., *Theor. Chim. Acta* **99**, 391 (1998).
27. Baerends, E. J., Bérces, A., Bo, C., Boerrigter, P. M., Cavallo, L., Deng, L., Dickson, R. M., Ellis, D. E., Fan, L., Fischer, T. H., Fonseca Guerra, C., van Gisbergen, S. J. A., Groeneveld, J. A., Gritsenko, O. V., Harris, F. E., van den Hoek, P., Jacobsen, H., van Kessel, G., Kootstra, F., van Lenthe, E., Osinga, V. P., Philipsen, P. H. T., Post, D., Pye, C. C., Ravenek, W., Ros, P., Schipper, P. R. T., Schreckenbach, G., Snijders, J. G., Sola, M., Swerhone, D., te Velde, G., Vernooijs, P., Versluis, L., Visser, O., van Wezenbeek, E., Wiesenekker, G., Wolff, S. K., Woo, T. K., and Ziegler, T., ADF 2000.02 Computer Code, 2000.
28. Espelid, Ø., and Børve, K. J., *J. Catal.* **195**, 125 (2000).
29. Becke, A. D., *J. Chem. Phys.* **98**, 5648 (1993).
30. Stevens, P. J., Devlin, F. J., Chablowski, C. F., and Frisch, M. J., *J. Phys. Chem.* **98**, 11,623 (1994).
31. Frisch, M. J., Trucks, G. W., Schlegel, H. B., Scuseria, G. E., Robb, M. A., Cheeseman, J. R., Zakrzewski, V. G., Montgomery, Jr., J. A., Stratmann, R. E., Burant, J. C., Dapprich, S., Millam, J. M., Daniels, A. D., Kudin, K. N., Strain, M. C., Farkas, O., Tomasi, J., Barone, V., Cossi, M., Cammi, R., Mennucci, B., Pomelli, C., Adamo, C., Clifford, S., Ochterski, J., Petersson, G. A., Ayala, P. Y., Cui, Q., Morokuma, K., Malick, D. K., Rabuck, A. D., Raghavachari, K., Foresman, J. B., Cioslowski, J., Ortiz, J. V., Baboul, A. G., Stefanov, B. B., Liu, G., Liashenko, A., Piskorz, P., Komaromi, I., Gomperts, R., Martin, R. L., Fox, D. J., Keith, T., Al-Laham, M. A., Peng, C. Y., Nanayakkara, A., Challacombe, M., Gill, P. M. W., Johnson, B., Chen, W., Wong, M. W., Andres, J. L., Gonzalez, C., Head-Gordon, M., Replogle, E. S., and Pople, J. A., Gaussian 98, Revision A.9, 1998.
32. Dunning, T. H., Jr., *J. Chem. Phys.* **90**, 1007 (1989).
33. Kendall, R. A., Dunning, T. H., Jr., and Harrison, R. J., *J. Chem. Phys.* **96**, 6769 (1992).
34. Woon, D., and Dunning, T. H., Jr., *J. Chem. Phys.* **98**, 1358 (1993).
35. Siegbahn, P. E., Blomberg, M. R., and Svensson, M., *Chem. Phys. Lett.* **223**, 35 (1994).
36. Siegbahn, P. E., Svensson, M., and Boussard, P. J., *J. Chem. Phys.* **102**, 5377 (1995).